Constraints on a shallow offshore gas environment determined by a multidisciplinary geophysical approach: The Malin Sea, NW Ireland

Xavier Garcia[1,2], Xavier Monteys[3], Rob L. Evans[4], and Michal Szpak[5]

[1]Barcelona Center for Subsurface Imaging, Institute of Marine Sciences, CSIC, Barcelona, Spain, [2]Formerly at Geophysics Section, School of Cosmic Physics, Dublin Institute for Advanced Studies, Dublin, Ireland, [3]Geological Survey of Ireland, Dublin, Ireland, [4]Department of Geology and Geophysics, Woods Hole Oceanographic Institution, Woods Hole, Massachusetts, USA, [5]School of Chemical Sciences, Dublin City University, Dublin, Ireland

Abstract During the Irish National Seabed Survey (INSS) in 2003, a gas related pockmark field was discovered and extensively mapped in the Malin Shelf region (NW Ireland). In summer 2006, additional complementary data involving core sample analysis, multibeam and single-beam backscatter classification, and a marine controlled-source electromagnetic survey were obtained in specific locations. This multidisciplinary approach allowed us to map the upper 20 m of the seabed in an unprecedented way and to correlate the main geophysical parameters with the geological properties of the seabed. The EM data provide us with information about sediment conductivity, which can be used as a proxy for porosity and also to identify the presence of fluid and fluid migration pathways. We conclude that, as a whole, the central part of the Malin basin is characterized by higher conductivities, which we interpret as a lithological change. Within the basin several areas are characterized by conductive anomalies associated with fluid flow processes and potentially the presence of microbial activity, as suggested by previous work. Pockmark structures show a characteristic electrical signature, with high-conductivity anomalies on the edges and less conductive, homogeneous interiors with several high-conductivity anomalies, potentially associated with gas-driven microbial activity.

1. Introduction

Gas-escape craters or pockmarks are common seabed features observed on continental margins and generally are associated with gas and fluid seepage. Pockmarks are known to be widely distributed in many basins around the World's oceans from coastal to deep water environments. Pockmarks have been observed in the North Sea [*Hovland*, 1984; *Hovland and Judd*, 1988], the Irish Sea [*Taylor*, 1992; *Yuan et al.*, 1992], the Scotian Shelf [*King and MacLean*, 1970], and in many other areas [*Josenhans et al.*, 1978; *Judd and Hovland*, 2007]. Studies of gas seeps are interesting from several perspectives including providing a better understanding of global methane budgets [*Judd and Hovland*, 2007], evaluating geohazards, investigating relationships between fluid flow processes and specific microenvironments created in the seafloor, often characterized by specialized microbiological activity, mineral precipitation, benthic fauna associations, as well as for their effects on water column dynamics.

Traditionally, pockmarks and shallow gas in marine sediments have been mapped using a range of acoustic tools (e.g., sidescan sonar, MBES, and subbottom profilers), optical devices (Underwater video, remotely operated vehicle (ROV)), and a range of seabed sampling techniques. This paper documents the pathways and presence of gas by using a combination of shallow EM data, high-frequency acoustics, and short sediment cores in a known shallow gas-bearing area. The combination of these various methods has allowed us to correlate the main geophysical signatures and some geological properties of the seabed, providing a unique approach for geohazard identification, multibeam seabed characterization, fluid migration paths, and sediment porosity.

There are very few EM surveys of areas affected by pockmarks [e.g., *Müller et al.*, 2011; *Minshull et al.*, 2012; *Hsu et al.*, 2014], but some of the conclusions drawn from these works are that shallow EM profiling can significantly improve understanding of sediment distribution and vertical zonation of seepage processes.

It has been postulated that the walls of pockmarks act as pathways for gas flow [*Newman et al.*, 2008] and that sediments are disturbed within the pockmark as a consequence of the violent gas release mechanism [*Judd and Hovland*, 2007]. Additionally, some studies show that bacterial activity feeding on gas in sediments can cause conductivity anomalies [*Atekwana et al.*, 2004; *Abdel Aal et al.*, 2010]. The present study is used to test whether EM methods can clearly detect pockmark signatures, the presence of gas within sediments, fluid release pathways and presence of bacterial activity.

2. Geological Setting of the Study Area

The Malin Deep Pockmark Field lies on the Irish continental shelf approximately 70 km offshore northwest Ireland (Figure 1). The area lies in the Malin Basin, situated in a complex structural setting, delimited to the north by the Stanton Banks fault and to the south by the Malin Terrace [*Dobson and Evans*, 1974; *Dobson and Whittington*, 1992]. The Skerryvore fault, a major normal fault, divides the study area into two different basins, the Donegal Basin and the West Malin Basin. The Donegal Basin extends parallel to the north coast of Ireland into the area of the Malin Sea with an east-northeast trend. The region is largely dominated by two structural trends, one NE-SW (Caledonian) and another almost orthogonal NNW-SSE trend (Paleozoic). Faults developed across this region in a NNW-SSE direction under a dextral strike-slip stress regime.

Igneous intrusions are common across the Malin Shelf including centers like the Malin Complex [*Riddihough*, 1968] and minor bodies on the Malin Trough closer to the study area. These intrusive bodies are generally subcropping the Quaternary material as part of relict structures from the successive erosional glacial events [*Dobson and Whittington*, 1992]. These intrusions are visible in the shallow seismic records and are marked by high-magnetic anomalies. In some instances, the instrusions outcrop at the seafloor and become visible in multibeam bathymetry [*Monteys et al.*, 2008]. These intrusions were initially detected
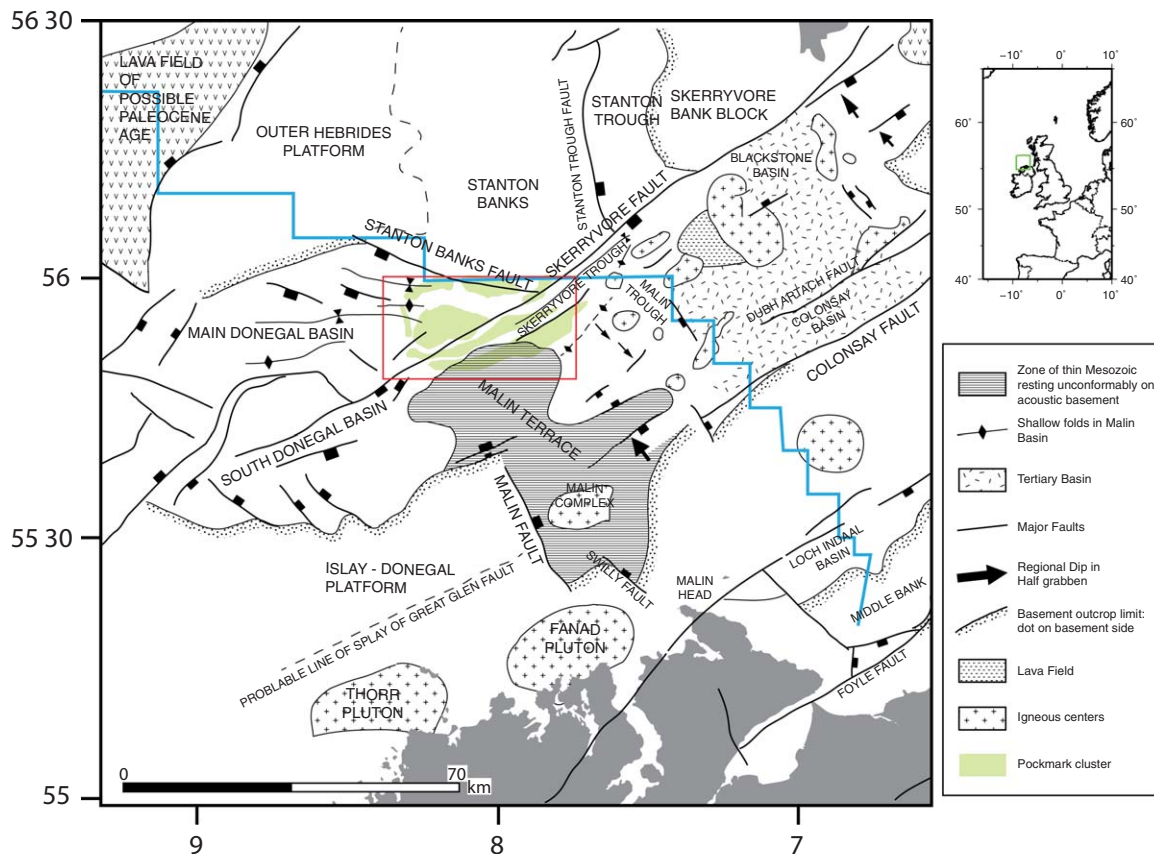

Figure 1. Geological sketch of the Malin Sea area after *Dobson and Whittington* [1992]. The red box indicates the study area, the Malin Deep Pockmark field. The light green patched areas around the study zone indicate the pockmark clusters in the Malin Deep (adapted from *Monteys et al.* [2008]). The light blue line indicates the limit of territorial waters between Ireland and the UK.

using magnetic surveys [*Riddihough*, 1968] and later dated by *Dobson and Whittington* [1992] as of Paleogene age features.

Quaternary sediments are recorded throughout the Malin Sea area with thicknesses varying from north to south from 175 to 125 m [*Evans et al.*, 1985]. The upper strata in the Malin Shelf is composed of marine glacial diposits and glacial landforms with bed forms alternating between sand patches and coarser sediments, ranging in size from pebbles to boulders to soft-layered Holocene silty muds in the study area [*Evans et al.*, 1985; *Dunlop et al.*, 2010]. The basin floor around the pockmark field is characterized by soft fine-grained sediment facies comprising more than 220 gas related pockmarks distributed in clusters around the main structural lineaments [*Monteys et al.*, 2008] (see also light green patched areas in Figure 1).

Hydrocarbons have been encountered in several of the northwest offshore basins, particularly those with thicker Permo-Triassic sequences. Hydrocarbon prospects rely on the existence of Carboniferous source rocks; however, Jurassic to Cretaceous source rocks have also been documented in the region. Paleogene reactivation of fractures may have allowed the leakage of reservoir hydrocarbons to the upper subsurface [*Parnell*, 1992].

3. Gas in Marine Sediments

Gas in marine sediments can have biogenic or thermogenic origin [*Floodgate and Judd*, 1992]. Biogenic gas is produced by the degradation of organic matter by bacterial activity at low temperatures, whereas thermogenic gas is produced by chemical reactions within the sediment in which time high temperatures and burial depth are important controlling factors [*Rice and Claypool*, 1981].

Free gas has an important effect on the acoustic properties of the seabed. Bubbles, even in small quantities, can cause markedly reduced compressional wave speeds, increased compressional wave attenuation, and increased sound scattering [*Anderson and Hampton*, 1980; *Wilkens and Richardson*, 1998; *Fonseca et al.*, 2002]. Free gas is also known to significantly alter sedimentary geotechnical characteristics, primarily by increasing seabed compressibility and reducing its undrained shear strength [*Sills and Wheeler*, 1992]. In the environmental sciences, gassy sediments are becoming increasingly important in global studies of climate change and methane budget [*Fleischer et al.*, 2001]. It has been suggested that methane fluxes associated with marine seepages have been greatly underestimated in the methane and carbon cycles [*Kvenvolden and Rogers*, 2005; *Milkov*, 2000].

Resistivity provides a first-order measure of seafloor porosity in sedimentary settings, allowing facies maps to be constructed or changes in lithology to be identified. In unconsolidated sediments, and to some extent in hard rock, porosity is a key parameter to understanding pore fluid and fluid transport (i.e., ionic concentration and mobility). The presence of gas (effectively an electrical insulator) will decrease the conductivity of the rock matrix because it may block or isolate the conductive water in the pores [*Ren et al.*, 2010]. Hydrates, like gas, are a resistive phase, and therefore, their effect on EM data is similar. *Yuan and Edwards* [2000] and *Schwalenberg et al.* [2005] report values of seafloor conductivity of 0.6–1 S/m in the absence of hydrates, and low anomalous conductivities ($<$0.2 S/m) in the presence of hydrates.

There is little information in the literature on the effects on conductivity of free or dissolved gas in sediments. Free gas would be expected to reduce effective porosity in a one-one basis as it effectively adds to the amount of resistive matrix. There is the possibility that gas could preferentially block key fluid connection pathways, and therefore, be more effective at reducing conductivity. Dissolved gas would change the seawater conductivity. *Börner et al.* [2013] report a decrease of conductivity as a result of dissolved CO_2 in sand saturated with saline water, although they also account for an increase of the conductivity caused by additional charges provided by the gas. However, this experiment was carried out at supercritical conditions and in the context of CO_2 sequestration.

However, the resistivity is affected to a much lesser extent than are acoustic properties [*Cheesman et al.*, 1993], which can suffer wipeouts in the presence of trace amounts of gas. *Schubel* [1974] demonstrated that only as little as 0.1% (v/v) of gas present in the sediment could reduce the speed of sound by a third. Moreover, gas acoustic signatures can vary greatly depending on factors such as: wavelength of acoustic pulse applied, distribution of gas in the lithofacies, and bubble size [*Judd and Hovland*, 2007]. Because of this extreme sensitivity, acoustic methods can detect gas but do not place constraints on gas volumes.

Therefore, the combination of different geophysical techniques, particularly seismic and electromagnetic methods, provides means of quantifying gas in situ. For more detailed information on relationship of conductivity, velocity, and gas see, e.g., *Wilt and Alumbaugh* [1998].

4. Material and Methods

4.1. Electromagnetic Data

The towed-electromagnetic (EM) system discussed in this paper consists of three main components, the deck electronics, a transmitter, and the receiver string. The seafloor components of the system (transmitter and receivers) form a 40 m long array, which is towed in contact with the seafloor at speeds of 1–2 knots.

The EM transmitter, a horizontal magnetic dipole, generates harmonic magnetic fields over a range of frequencies (200–200 kHz), and the three receivers, tuned to measure the magnetic fields propagating through the ambient seawater and seafloor, are towed at fixed distances behind (4, 12.6, and 40 m). At a given frequency, the strength of magnetic fields decays away from the transmitter as a function of the conductivity of the seafloor (i.e., according to the skin depth), decaying more rapidly in more conductive media. The sensitivity of the magnetic dipole-dipole system, along with the physics of the propagation of the fields through the seafloor was presented in *Cheesman* [1989]. Further details of the system, sensitivity, data processing, and inversion are given in *Evans* [2007], and details on resolution can be found in *Evans* [2001]. The noise level of the system has been estimated to be on the order of 1% in terms of apparent porosity [*Evans et al.*, 1999]. As a first-order approximation [*Evans et al.*, 1999], the depth of penetration of a receiver is about one-half of the receiver-transmitter separation (i.e., the 40 m receiver is sensitive to the electrical properties of the top 20 mbsf). Since the 4 m receiver failed to collect any data, we will refer below to the 40 m receiver as the deeper receiver and to the 13 m receiver as the shallow receiver.

Because the system maintains a fixed distance between source and receiver, it can be regarded as a mapping tool. In order to build up a map of subseafloor structure, only relatively spatial sparse coverage is needed [*Evans et al.*, 1999]. Archie's law [*Archie*, 1942] can be used to obtain estimated porosities for a simple two-phase system that contains a conductive pore fluid. In fully water-saturated rocks, Archie's law can be expressed [*Evans*, 2007]:

$$\phi = \alpha^{1/m} \tag{1}$$

where ϕ is the porosity, m is the cementation factor, and α is the conductivity contrast defined as the ratio between grain matrix conductivity and pore fluid conductivity. The cementation factor can be obtained from laboratory analysis and varies between 1.5 and 3 [*Jackson et al.*, 1978, 1998]. A more complete form of Archie's law than equation (1) in which gas saturation is taking into account:

$$\sigma_{sediment} = \phi^m (1 - S_g)^n \sigma_{water} \tag{2}$$

where σ indicates electrical conductivity, ϕ porosity, m the cementation factor, and n the saturation exponent. The saturation exponent models the effect of the presence of nonconductive fluids (usually hydrocarbons). The effect of the saturation term in Archie's law is a drop in conductivity, but without any precise knowledge of the gas saturation can be misinterpreted as a change in porosity.

The resulting maps provide superior spatial coverage than conventional coring techniques and porosities, obtained from conductivities using equation (1), in regions where coring techniques fail to recover samples, but more importantly provide a means of interpolating between discrete core locations. Finally, the combined methodology provides estimates of physical properties where seismic reflection profiles are contaminated by strong bottom multiples or signal starvation due to the presence of methane gas [*Cheesman et al.*, 1993]. The system is, however, perfectly complementary to seismic methods and is best used in concert with high-resolution seismic reflection techniques which define the stratal geometry, and from multichannel seismics velocities and therefore densities, while the EM data define the electrical properties and from those porosities [*Evans and Lizarralde*, 2003]. *Szpak et al.* [2012] have reported the application of this system in the Malin Deep.

4.2. Bathymetry

Bathymetry data were collected in 2003 as part of the Irish National Seabed Survey, a 7 year multidisciplinary baseline-mapping program [*Dorschel et al.*, 2011]. Data were acquired on board the R/V Celtic Explorer using a Kongsberg-Simrad EM1002 multibeam echo sounder, with an operational frequency of 93–98 kHz and pulse length of 0.7 s. Additional EM1002 S multibeam data used in this research were collected in 2006, coinciding with the EM survey on board the R/V Celtic Voyager. These multibeam lines were acquired at a shorter pulse length (0.2 s), at very low survey speed (2–3 knots), and were primarily used for multibeam echo sounder (MBES) backscatter-EM analysis [*Garcia et al.*, 2007].

4.3. Subbottom Profiler

Subbottom profile (SBP) data were acquired using a heave-corrected SES Probe 5000 3.5 kHz transceiver in conjunction with a hull-mounted $4° \times 4°$ transducer array. Acquisition parameters, data logging and interpretation were carried out using the CODA Geokit suite. Both Raw Navigation string and Heave Compensation string were fed into the Coda DA200 system (from the Seapath 200). An average estimated acoustic velocity of 1650 m/s was used to calculate the thickness of the sedimentary units. Acoustic penetration in some areas was on the order of 60 m below the seabed, with approximately 0.4 m resolution. Full acquisition parameters are detailed as follow: Trigger (variable, up to 350 ms); sweep time (variable, up to 349 ms); Delay (variable, up to 100 ms); frequency (3.5 kHz); TVF "Band Pass" (Low = 2000 Hz, High = 5000 Hz).

4.4. Shallow Sediment Cores

A number of shallow cores were made available for this study. In 2008, on board the R/V Celtic Explorer, two 6 m long cores were obtained, using a vibrocorer, in the vicinity of pockmark 2: core CE08_044 was located outside the pockmark and core CE08_045 was taken inside the pockmark (Tables 1 and 2 and Figure 2). The cores were cut into 1 m sections and kept in cold storage on board. The cores presented a hydrogen sulfide gas odor during the cutting, and two sections from CE08_044 showed the presence of bubbles during the sealing (sections 4 and 6 in Figure 3). These two cores were scanned at 1 cm intervals (as whole core and split) for physical properties using a Multiscanning Core Logger (MSCL) MSCL scanner

Table 1. Mean and Median of Particle Size Analysis of CE08_044 Core (Outside Pockmark)

Sample Name	Clay (<2 μm) %	Silt (2–63 μm) %	Sand (63–2000 μm) %	Mean Grain Size	Sorting	Skewness
5	3.75	88.06	8.20	28.89	1.58	0.20
20	3.94	89.86	6.20	26.02	1.54	0.16
40	3.65	88.31	8.04	29.21	1.56	0.26
60	3.55	88.39	8.06	28.75	1.57	0.23
80	3.74	88.34	7.92	27.90	1.59	0.18
100	3.34	84.23	12.43	35.50	1.66	0.24
120	3.26	87.52	9.22	21.23	1.57	0.30
140	3.65	85.36	10.98	31.03	1.62	0.29
160	2.24	77.04	20.72	44.08	1.60	0.68
180	1.69	70.16	28.15	52.70	1.54	0.96
200	1.66	71.75	26.60	51.14	1.53	0.94
220	1.72	70.87	27.41	52.03	1.53	1.00
240	1.39	69.98	28.63	54.50	1.43	1.18
260	1.48	73.48	25.03	50.52	1.44	1.07
280	2.78	86.48	10.74	33.37	1.54	0.76
300	3.37	89.72	6.91	27.26	1.51	0.34
320	7.54	84.37	8.09	27.84	2.04	1.30
340	3.01	86.23	10.76	32.18	1.57	0.41
360	6.28	85.73	7.99	29.32	1.85	1.20
380	9.71	82.84	7.45	25.89	2.14	1.17
400	13.86	82.76	3.39	18.33	2.22	1.04
420	13.71	80.10	6.19	21.27	2.34	0.91
440	14.12	80.49	5.39	20.29	2.34	0.97
460	12.36	80.45	7.19	24.14	2.32	0.89
480	13.59	79.73	6.68	46.63	2.52	0.41
500	13.19	82.90	3.91	19.61	2.22	0.93
520	16.34	79.51	4.15	18.89	1.89	0.20
540	16.81	79.22	3.97	19.38	1.91	0.17
560	18.65	78.72	2.63	15.29	1.82	0.10
Mean	7.05	81.81	11.14		1.80	
Median	3.74	82.84	8.04		1.60	
Std dev	5.63	6.07	8.20		0.33	

Table 2. Mean and Median of Particle Size Analysis of CE08_045 Core (Inside Pockmark)

Sample Name	Clay (<2 μm) %	Silt (2–63 μm) %	Sand (63–2000 μm) %	Mean Grain Size	Sorting	Skewness
5	4.63	86.36	9.01	28.89	1.70	−0.25
20	13.77	83.90	2.33	15.46	2.18	1.10
40	12.00	82.76	5.24	33.23	2.32	0.60
60	2.04	59.96	38.00	88.46	2.03	0.30
80	13.49	78.16	8.35	66.35	2.70	0.15
105	13.21	81.78	5.02	24.02	2.35	0.89
120	13.70	80.89	5.41	22.36	2.37	0.89
140	14.55	80.09	5.35	37.17	2.49	0.53
160	4.66	89.92	5.42	23.48	1.57	−0.22
180	13.14	80.16	6.70	55.46	2.58	0.26
200	15.42	77.86	6.73	69.44	2.78	0.06
205	13.94	83.43	2.63	15.70	2.22	1.11
220	10.09	86.99	2.92	17.52	1.98	1.00
240	13.05	81.77	5.18	25.21	2.36	0.81
260	5.29	91.30	3.41	18.07	1.47	−0.19
280	12.56	82.93	4.51	21.76	2.25	0.93
300	10.30	85.04	4.67	21.16	2.11	0.96
320	5.53	93.75	0.72	13.39	1.29	−0.13
340	8.12	89.13	2.75	17.61	1.76	0.83
360	4.58	93.80	1.62	15.25	1.33	−0.16
380	15.10	82.51	2.39	17.12	2.32	1.07
400	15.54	81.71	2.76	15.58	2.33	1.09
420	13.91	82.04	4.05	18.83	2.31	1.03
440	13.66	83.27	3.07	16.36	2.24	1.12
460	14.93	82.82	2.25	16.71	2.28	1.04
480	14.05	80.12	5.83	22.51	2.41	0.93
500	13.66	84.19	2.15	15.50	2.14	1.10
520	18.59	79.50	1.91	14.17	2.40	1.02
540	18.38	79.19	2.44	15.14	2.39	0.94
560	17.24	80.28	2.48	16.24	2.41	0.99
575	17.00	81.07	1.93	14.33	2.33	1.06
Mean	12.13	82.80	5.07		2.17	
Median	13.66	82.51	3.41		2.31	
Std Dev	4.42	5.98	6.43		0.37	

(Geotek) in Boscorf (Southampton National Oceanographical Center). The MSCL scanner calculates a series of physical parameters like magnetic susceptibility, X-ray fluorescence (XRF), density, electrical conductivity, and P velocity from cores. Particle size analysis at 20 cm intervals was performed using a Malvern Mastersizer-S bench top laser granulometer. Pore waters were analyzed at the chemistry laboratory in Dublin City, and the results were presented in detail in *Szpak et al*. [2012]. Physical analysis results are summarized in Tables 1 and 2 and Figures 3a and 3b. In 2006, five gravity cores (3 m long) were obtained on the same cruise as the marine EM data described in this work (some of the triangles in Figure 2) and other gravity cores were obtained during later cruises. Sediment cores were described and particle size analysis performed at specific intervals. These additional cores are all located outside the pockmark area and were used qualitatively to characterize the uppermost sediments [*Szpak et al*., 2012].

5. Results

5.1. Sediment Core Results

The results from the two 6 m sediment cores taken in 2008 are presented in Tables 1 and 2 and Figures 3 and 4. Cores CE08_44 and CE08_45 present similar characteristics in their composition and overall physical properties, allowing characterization of the upper most 6 m as soft homogenous fine-grained sediments from very fine sands to silts. However, both cores show significant differences in stratigraphic structure. Inside the pockmark (Table 1), core CE08_45 has a generally homogeneous appearance and a lack of clearly defined structure or sedimentary units with only minor fluctuations in silt/clay ratio. Physical properties logs and grain size analysis reflect the homogeneity with fairly constant measurements, narrow variations and no clearly visible primary trends (upward increasing or decreasing trends). Grain size profiles in the upper 3.7 m indicate a structureless sedimentary sequence; while in the lower part sediment grain size patterns contain distinct gradients (Figure 4). This is not the case for the core outside the pockmark (CE08_44, Table 2 and Figure 3). Here the uppermost 6 m of sediments show clear internal structure, and the physical properties
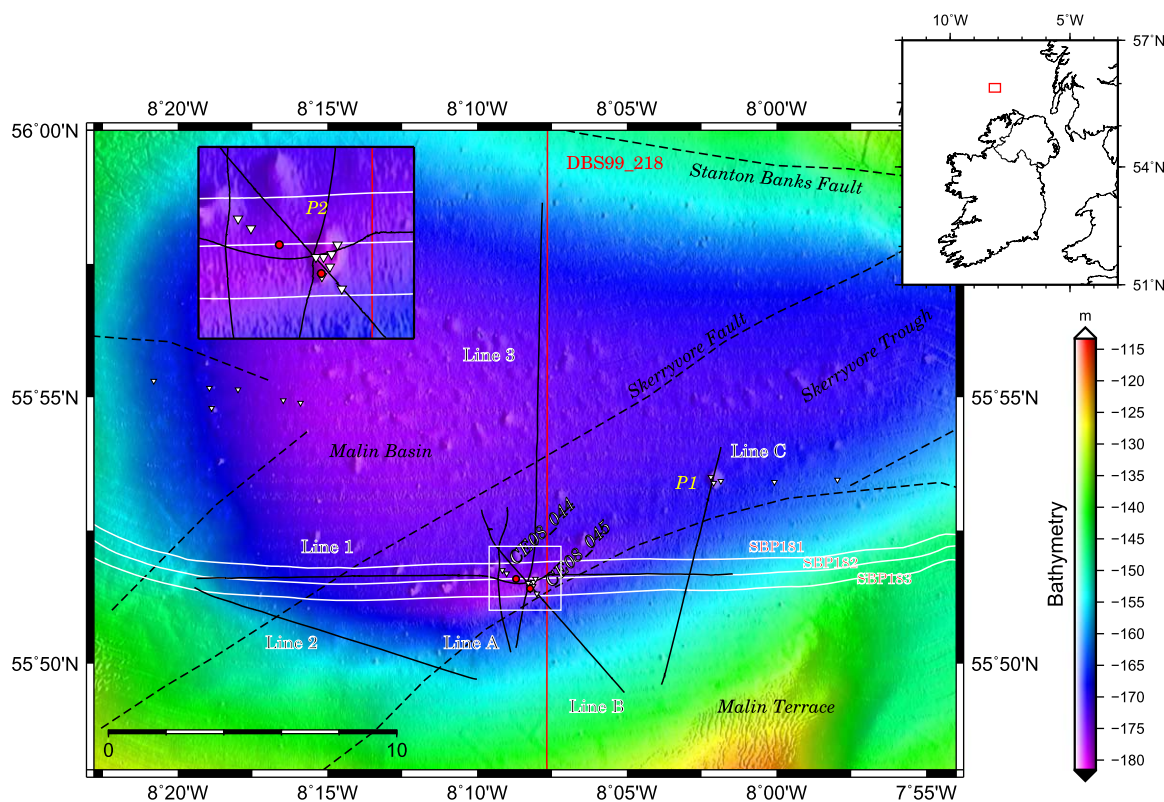
Figure 2. Bathymetric map with EM lines (black), subbottom profiler data (white) and seismic reflection data (red). The location of vibro-cores (red dots) and samples and gravity cores (white triangles) is also indicated. The inset plot on the top left side of the figure is a zoom to the area marked by presence of Pockmark 2 (white box) where the activities of this study were mostly concentrated. Dashed lines indicated main faults and tectonic units.

and grain size confirm the presence of primary trends and a gradual transition within the units, which are also clearly visible in the subbottom profiles. It is also noticeable a distinctive layer between 1.5 and 3 m below the seafloor (shaded area in Figure 4), which is dominated by fine sand with an almost total absence of clay (<2%). Physical analyses show an increase of density, P wave velocity and resistivity, and a decrease of the fractional porosity corresponding to this layer. Focusing on the first meter of the core values, the mean grain size within the pockmark is 46.5 μm while outside the pockmark is 29.4 μm (Tables 1 and 2).

5.2. Geophysical Data

The EM survey consisted of six lines, maximizing coverage of the area and passes over gas charged seafloor and particularly large composite pockmarks (Figure 2). The data are presented in Figures 5–10 as apparent conductivities from half-space inversions of the apparent resistivity data from each receiver. The final errors in fits of the model to the observations were below 2% except a few locations where errors were around 3%. The apparent conductivities were visually inspected for anomalous data points like spikes or areas in which there was no alignment between transmitter and receiver, and those sections were removed.

Line 1 crosses the basin following an approximate EW transect and is coincident with a 3.5 kHz pinger sub-bottom profile (Figure 5); line 2 is located on the southwestern slope of the basin; line B runs in SE-NW direction across the basin; and lines 3, A and C in NS direction. In all cases, the bathymetry in included as a visual reference to some of the features or to indicate the situation of the profiles within the basin.

In earlier surveys, using this EM system, the apparent conductivities were converted to apparent porosities [e.g., *Evans et al.*, 1999; *Evans and Lizarralde*, 2003] using Archie's law (equation (1)), using an assumed value of the cementation factor based on complementary data. Our study area is affected by changes in facies and also gas, and so to do a proper estimation of the porosity, extensive coverage by ground samples would be required. We therefore, we present results as apparent conductivities.

An existing seismic line and three subbottom profiles have also been used in the present work. These data were processed following standard procedures discussed earlier.
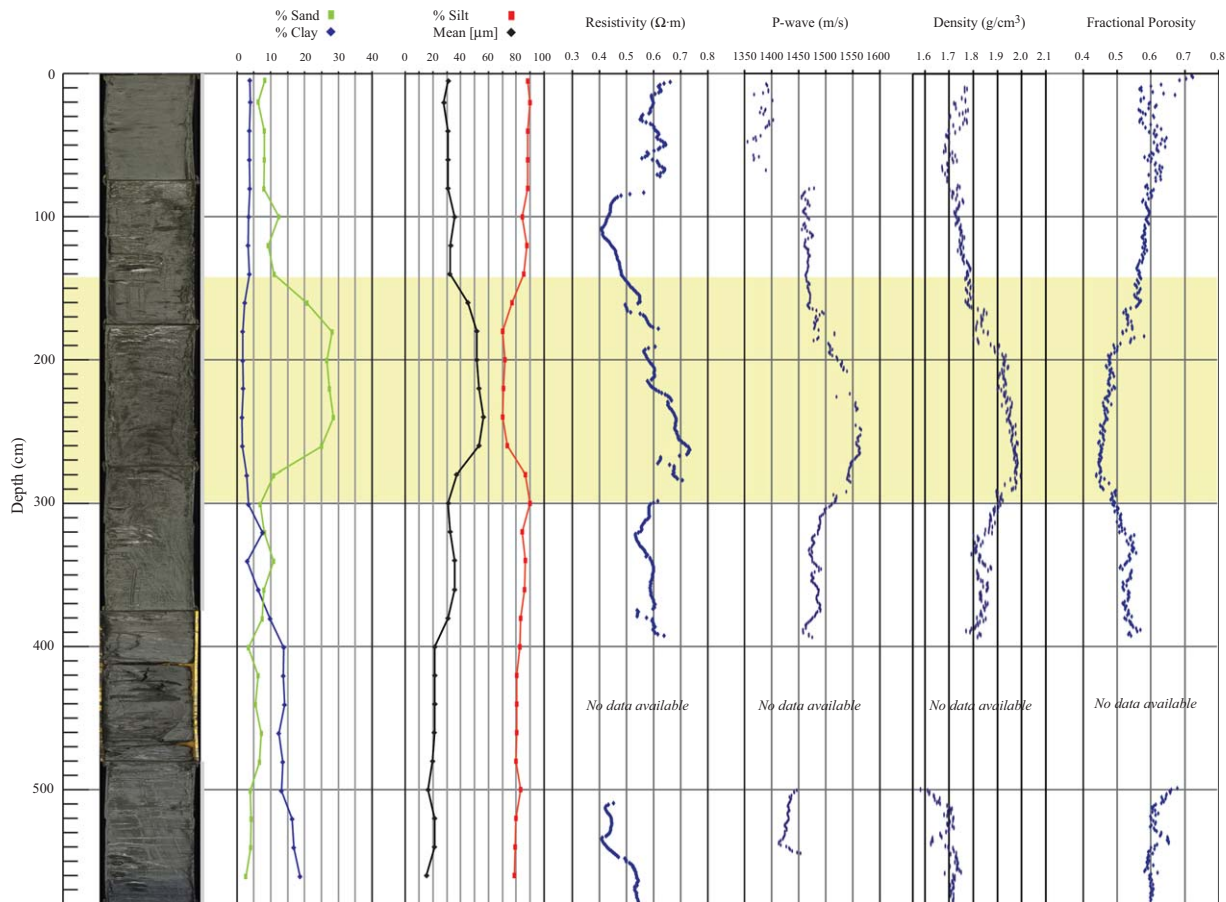
Figure 3. Core results from CE08_044. Image, PSA, and physical properties of core outside pockmark P2.

5.2.1. Line 1

At 19 km, line 1 (Figure 5) is the longest profile in our survey. The line starts on the Eastern side of the basin, on the northernmost edge of the Malin Terrace, and finishes on the western part of the Malin basin, toward the Donegal basin. Apparent conductivities along the profile vary between 0.9 and 1.2 S/m. On the eastern end (region E), differences in apparent conductivities of up to 14% between the two receivers suggest an overall downward coarsening of the lithological units. This is followed by a positive conductivity trend (region D) in both receivers, indicating finer sediments as the instrument moved to the central part of the basin. At about 5 km from the beginning of the profile (region C), conductivities decrease and become more irregular, reflecting greater lateral structure in the subsurface.

One of the most interesting features in line 1 is located 7.5 km from the beginning of the profile (region C). The overall conductivities of the upper 20 m (sensed by the deeper receiver) are higher than the conductivities of the top 6 m (as sensed by shallower receiver) of seafloor. The data in this area are poorly described by a half space, indicative of laterally heterogeneous media under the receiver. This region has a significant acoustic signature in the subbottom profiler (Figure 5, bottom), and is also coincident with a magnetic anomaly (data not shown) that has been interpreted as an intrusive body located at some 18 mbsf. As the system crossed the area affected by this igneous intrusion, the conductivity on the 40 m receiver rapidly increased, showing larger values than the shallower receiver. Additionally, the acoustic records showed an increase of the thickness of Unit 1 and acoustic blanking (AB labels on Figure 5, bottom plot). As the system moved west, conductivity values decreased.

Pockmark 2 (P2 in Figure 5) is imaged clearly by both receivers, although with an opposite behavior. Conductivities recorded by the deeper receiver decrease while those on the shallower receiver increase. Anomalous spikes in conductivity are seen at the edges of the pockmark that we discuss later.
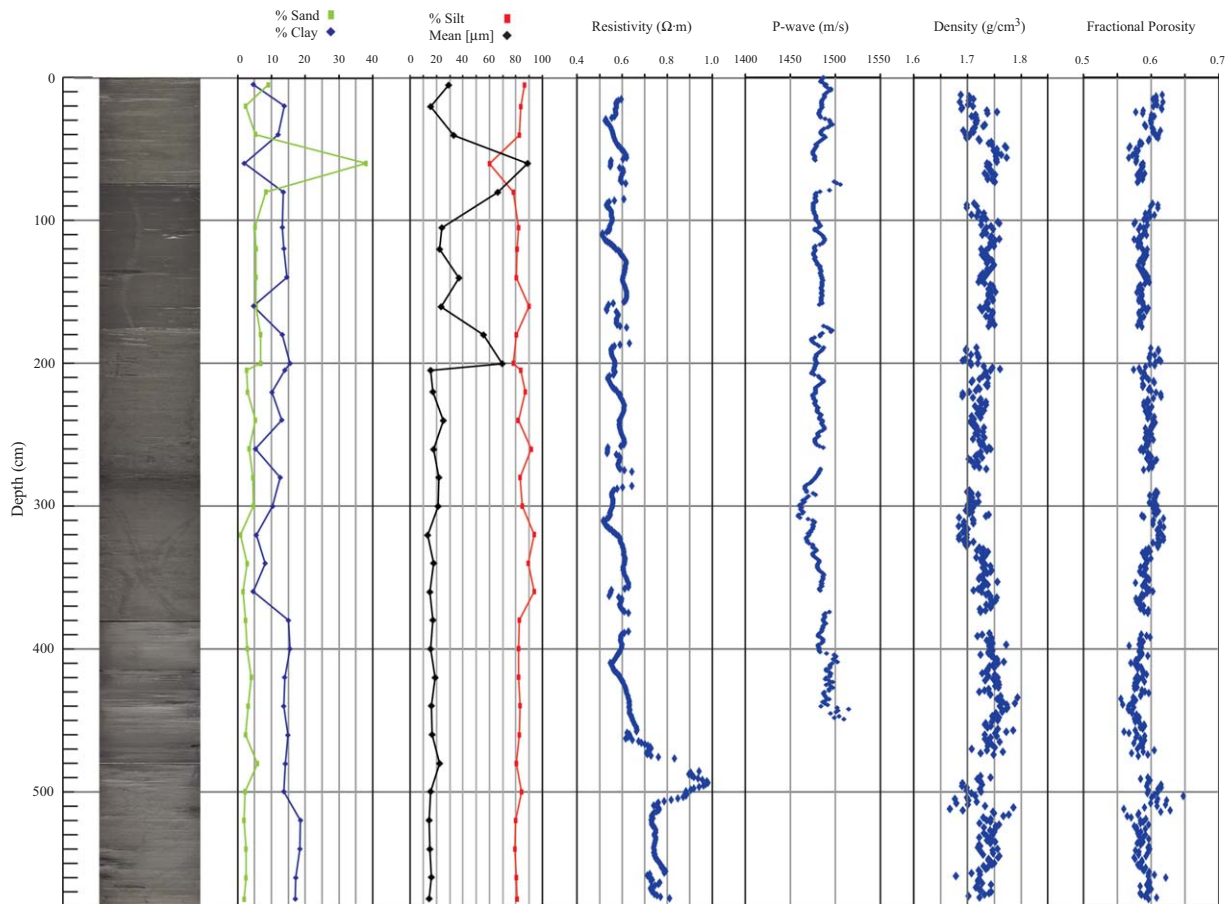
Figure 4. Core data CE08_045. Image, PSA, and physical properties of core inside pockmark P2.

Detailed examination of the conductivity profile in region C (Figure 5) shows a complex structure as the system enters a small pockmark (labeled SP). Within the pockmark, the two receivers show opposite behavior (increase for shallow receiver and decrease for deeper receiver) suggesting a steeper conductivity gradient within the pockmark itself. Past this pockmark, toward the West, the conductivities regain the regional trend and increase in magnitude. *Szpak et al.* [2012] have described in detail the EM properties of the seafloor within this composite pockmark (P2).

Toward the western part of the line (region B), conductivity decreases gradually, punctuated by several sharp decreases, with both profiles finally converging to the same values suggesting a thick and homogeneous unit (region A, Figure 5), clearly seen in the subbottom profiler data.

On the eastern side of the basin, regions D and E show a decrease in conductivity. Within region D, the conductivity profiles on both receivers show similar trends, similar to those in region B, although the shallow seismic unit 1 is thicker in region D and there is an obvious difference in conductivity values, caused by the difference in stratigraphy. Responses in region E are more influenced by the thinning of units 2 and 3 (see shallow seismics in bottom plot).

Subbottom profiler line 182 (Figure 5, bottom plot), shows a regional topmost unit (unit 1), which is generally well and closely stratified, with parallel reflectors from horizontal to gently inclined. This unit has a thickness ranging from a few meters at the basin edge to over 40 m in the central part of the basin. The unit is locally disturbed under pockmarks or adjacent to near-surface subcrops. The bottom part shows bedding planes that are in places gently folded or inclined and some accommodation structures. Unit 1 lies semiconformably above Unit 2.

Both Units 1 and 2 correspond to the Jura and Barra formation [*Dobson and Whittington*, 1992], which can be traced beneath the upper unit on most records. In general, unit 2 exhibits a structureless and
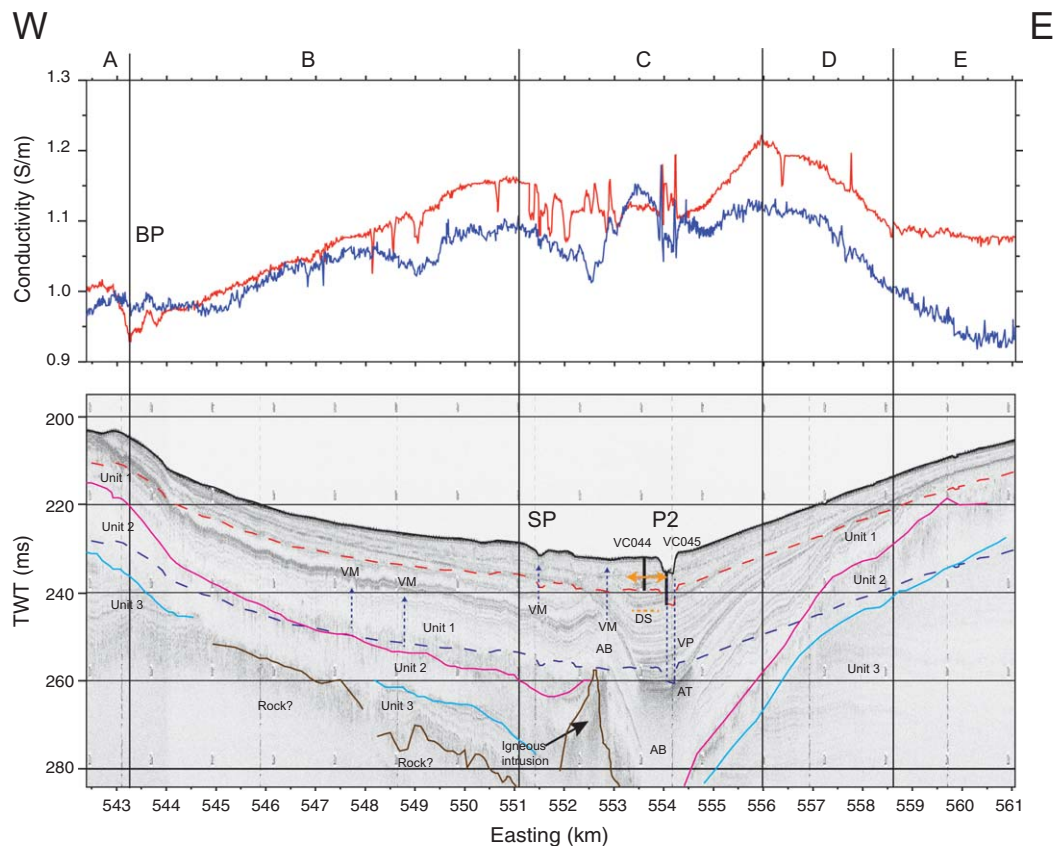
Figure 5. (top) EM line 1 showing conductivities, colored according to receiver sensitivity depth (red: 6 mbsf; blue: 20 mbsf). (bottom) Sub-bottom profiler (3.5 KHz) seismic line 182, aligned with the EM line. Lines blue and red on bottom plot indicate 6 and 20 mbsf depths to match depth of sensitivity of EM receivers. P2: Pockmark 2. SP: Small pockmark. BP: Buried pockmarks. AT: Acoustic turbulence. AB: Acoustic blanking. DS: Distorted sediments. VM: vertical migration pathways, also vertical dark blue dashed lines.

semitransparent acoustic character throughout the entire basin, with minimal internal reflectors and low backscatter response. Thickness is relatively uniform throughout the basin, averaging 5–15 m, thinning to the edges (Figure 5). Some infrequent internal reflectors appear as enhanced isolated reflectors and in other places like vertical plume-like structures (possibly fluid migration paths, labeled VM dashed blue lines).

Unit 3 underlies this unit with a pronounced erosional surface. This unit appears discontinuously in the pinger records because it is located in the limit of the acoustic penetration. In contrast to unit 2, unit 3 appears well and closely stratified, with inclined or folded parallel reflections.

Gas anomalies in the basin have been reported in *Monteys et al.* [2008] and *Szpak et al.* [2012]. Acoustic data (Figures 5 (bottom plot) and 11) reveal that there is widespread evidence of shallow gas-disturbed sediments, particularly within the unit 1. Features such as reflector blanking and amplitude enhancement, commonly referenced as indicators of shallow gas, can be observed throughout the area and are not limited to cooccurrence with pockmarks. Fluid migration pathways are present in the records and are most commonly observed within the unit 1 sections. They appear as vertical hyperbolic anomalies across strata (meter scale), suggesting vertical migration, or parallel-to-strata signal enhancements indicative of lateral fluid flow (extending up to hundreds of meters). On close inspection in the vicinity of the largest pockmarks, vertical fluid migration pathways resembling chimneys can be observed immediately below the pockmark units with a width of approximately 50 m. Acoustic turbidity facies and disrupted strata can be observed below the largest pockmark (P2), indicating a correlation between the acoustic gas facies and the seabed depressions (Figures 5 and 11). Similarly disturbed strata are evidence of recent migration of gas through the seabed. Finally, hydroacoustic evidence of gas seeping or gas plumes has not been observed in the pockmark area, thus it is unclear whether these features are only periodically active or are completely inactive.
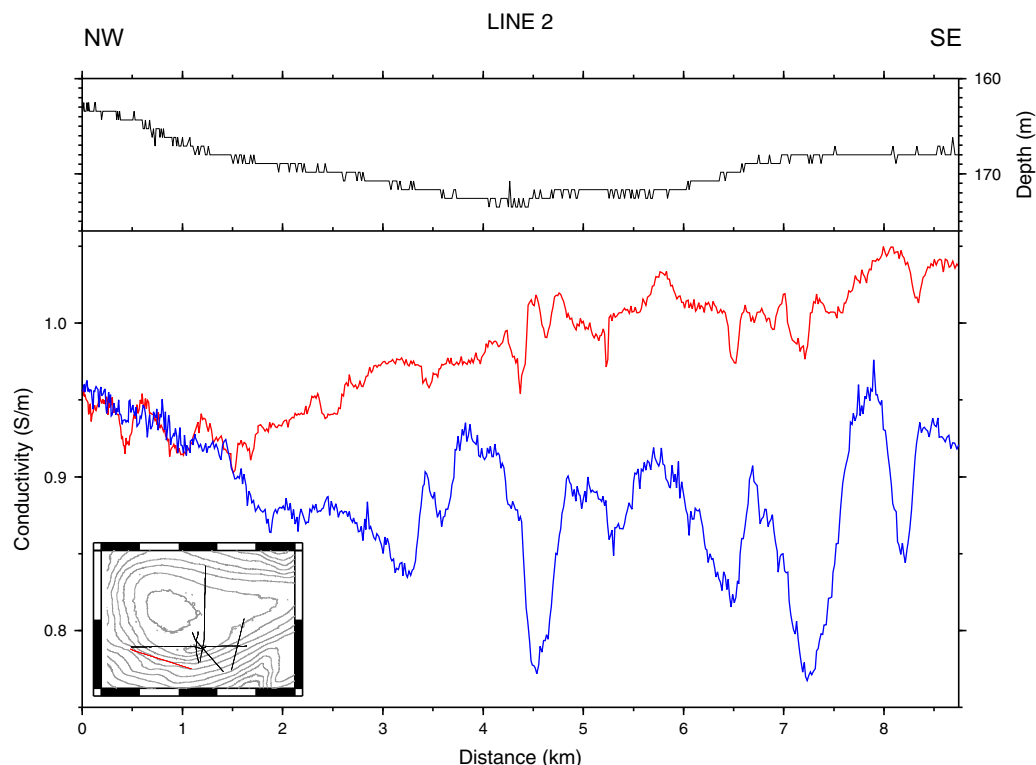
Figure 6. EM line 2 showing conductivities, colored according to receiver sensitivity depth (red: 6 mbsf; blue: 20 mbsf). (top) Bathymetry measured from CTD sensor in EM system.

Locally, depressions within the unit 1 strata (Figure 5, feature BP) resembling the ones on the seabed have been observed across the basin. Some of these features are coincident with conductivity signatures typical of gas-disturbed sediments that we observed at other locations in the study region: raised edges and reduced conductivity, suggesting that these features are likely a series of buried pockmarks. Feature BP also results in measured conductivities that are larger on the deeper receiver than on the shallower one.

Gas related anomalies around Pockmark 2 appear to be concentrated in the vicinity of a series of igneous intrusions. These Paleogene intrusions appear to have facilitated gas migration to the seabed providing near-vertical planes through several units disrupting the parallel strata (Figure 5, region C).

5.2.2. Line 2
Line 2 (Figure 6) runs along the southwestern side of the basin and is the only line that does not cross the basin itself. For the first 1.5 km, the conductivities of both receivers are similar, suggesting that there is a thinning of the uppermost unit. After this point both receivers show very different behavior, with the shallower receiver showing smoothly varying conductivities that are about 1 S/m, considered the normal value for unconsolidated sediments [*Yuan and Edwards*, 2000]. The deeper receiver measures large variations that are related to changes in the second unit and thus caused by structural (lithological and porosity) changes, with areas related to larger conductivity values corresponding to areas of the thicker upper unit.

5.2.3. Line 3
As a whole, line 3 (Figure 7) shows similar responses to those on the other lines collected. The line starts outside the basin where conductivities are relatively low. As the instrument moved into the deepest part of the basin, conductivities started to rise and 2 km from the beginning of the profile, when crossing over pockmark 2, conductivities plateau within a very homogeneous area (2 km long) at about 1.25 S/m. This area is coincident with region C as noted in Figure 5. After this area, conductivities decrease gradually toward the north with the exception of a dome-like pattern of ca. 3 km (feature X in Figure 7), although toward the northern edge of the basin there is an area where conductivity anomalies decrease and display higher amplitude variations for the shallow receiver. This section coincides with an area affected by gas escape features in the acoustic records (see pockmark cluster locations in Figure 1). The fairly parallel
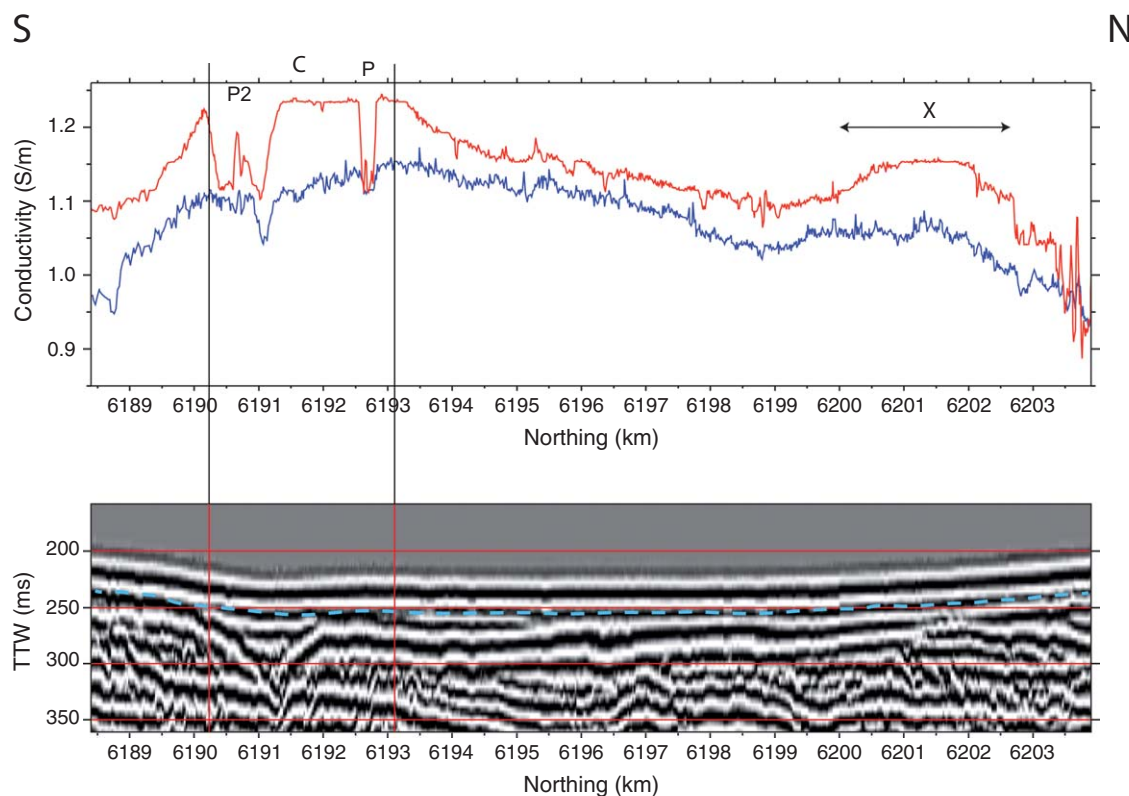
Figure 7. (top) EM line 3 showing conductivities, colored according to receiver sensitivity depth (red: 6 mbsf; blue: 20 mbsf). (bottom) Top 350 ms from 2-D multichannel seismic reflection profile DBS99_128, blue line indicates 40 ms TWT below the seafloor, corresponding to some 20 mbsf depth. Seismic data sampling rate of 1 ms. The data were processed using prestack time migration and normalized stack. Posteriorly it was band-pass filtered with low cut at 3.5 Hz and high cut at 309 Hz.

distribution of conductivities measured by both receivers, indicate that both are imaging similar geological facies (composed of a number of layers) with downward decrease of porosity by sediment compaction.

Unfortunately, there was no shallow seismic data coincident with this profile, but there is a reflection seismic line (DBS99_218) along an adjacent parallel track to the EM line. The bottom plot of Figure 7 shows a zoom in image of the first 350 ms of this seismic line DBS99_218. The plot shows the shallow stratigraphy of the study area down to some 70 mbsf (almost 200 mbsl). The top section of the basin shows a very distinctive parallel layering in the unconsolidated sediments in the top 60 m section. There is a channel-like feature 80 m below the pockmark 2 area and coincident with the splay of the Skerryvore Fault. This interval largely correlates with area C, generally characterized by high-conductivity values and low anomalies. Interestingly, two coincident negative conductivity anomalies are seen in both profiles in this area (from 6198 to 6199 km), which correspond to the channel-like feature and that we interpret as possible gas migration pathways (11). Perhaps one important observation is that the shallow stratigraphy remains near horizontal and parallel toward the North of the profile where the EM data show more variability. This disparity between data sets as we will discuss later is likely caused by the presence of gas in sediments. Unfortunately the conventional seismic data (Figure 7) do not have sufficient resolution in the shallower sections to show any changes.

5.2.4. Line A

Line A (Figure 8) is the shortest profile of our survey. It roughly follows a NS line across the basin about 1.5 km west of line 3 and pockmark P2 (Figure 2). The conductivity profile along line A, in the area where it crosses line 1 shows an anomalous area located at about 1.5 km from the beginning of the profile, which is also seen along line 1, likely caused by the presence of the igneous intrusion. According to the shallow EM receiver (upper 6 m), this area is characterized by a sharp decrease in the conductivity (between 1.8 and 3 in profile), which we interpret as a very large but shallow pockmark (about 1 km long by some 2 m depth expression in bathymetry), which has been eroded and partially infilled by sediments. The deeper EM
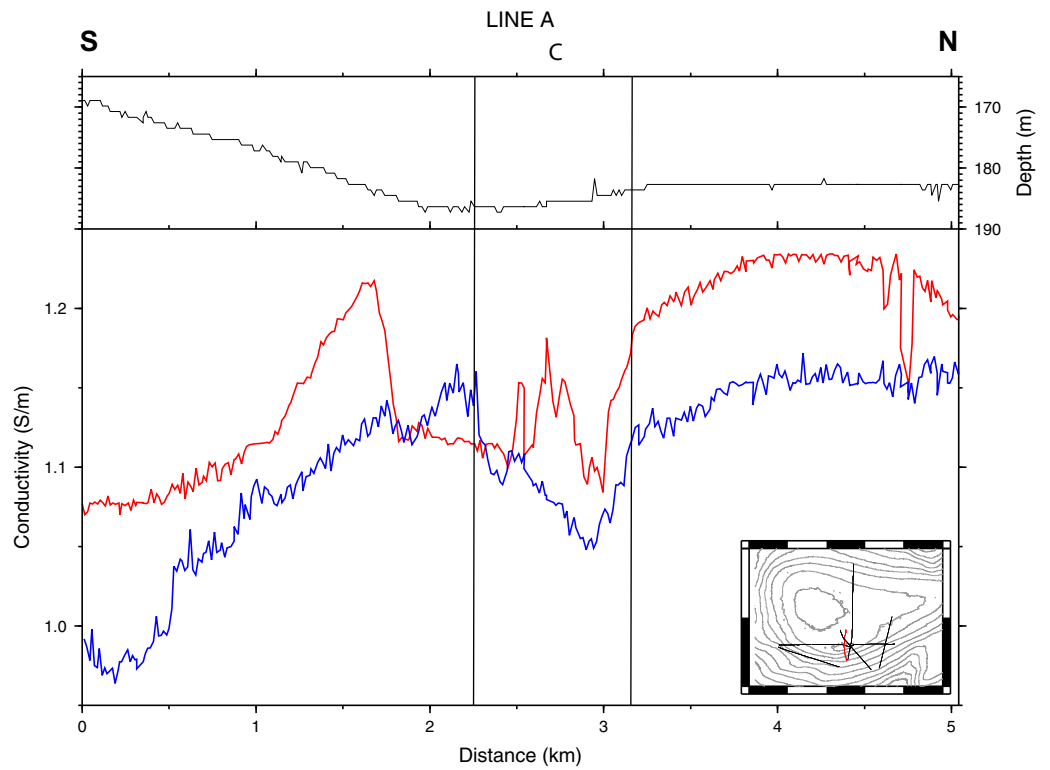
Figure 8. EM line A showing conductivities, colored according to receiver sensitivity depth (red: 6 mbsf; blue: 20 mbsf). (top) Bathymetry measured from CTD sensor in EM system.
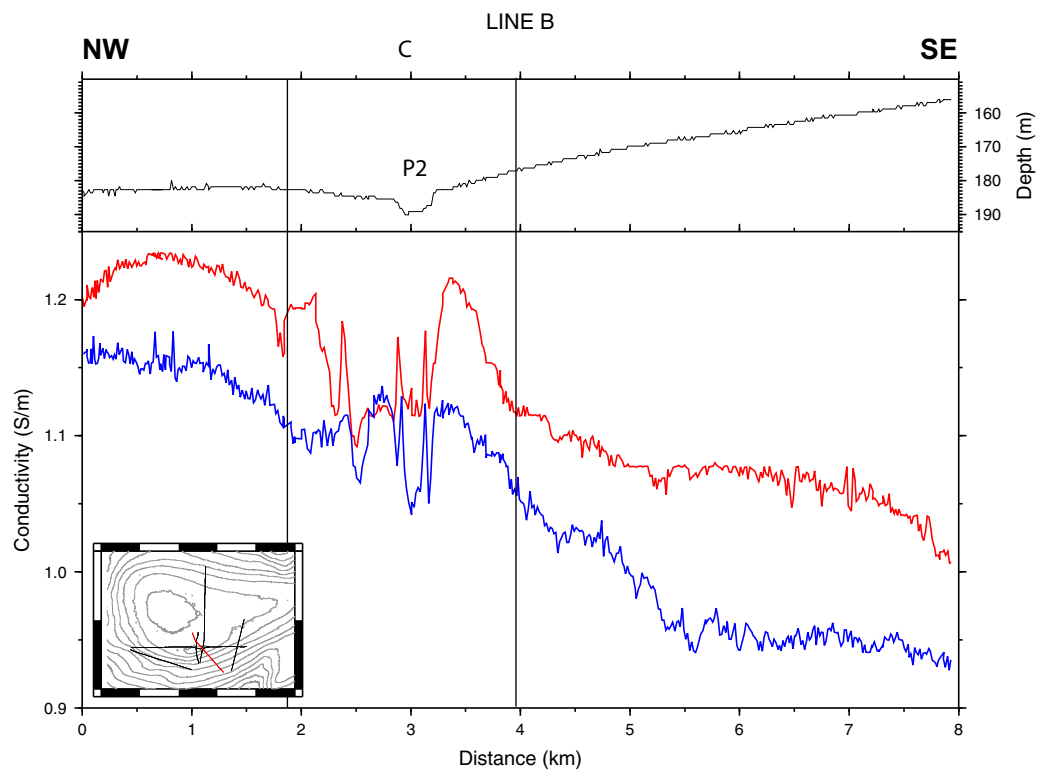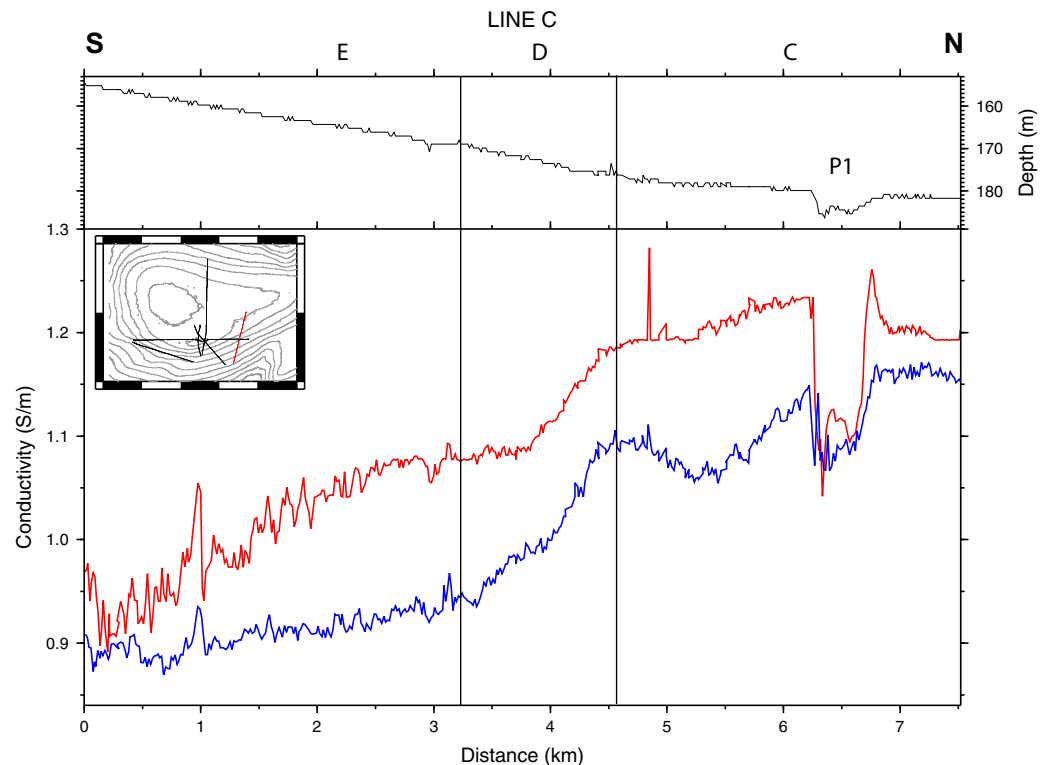

Figure 9. EM line B showing conductivities, colored according to receiver sensitivity depth (red: 6 mbsf; blue: 20 mbsf). (top) Bathymetry measured from CTD sensor in EM system.

Figure 10. EM line C showing conductivities, colored according to receiver sensitivity depth (red: 6 mbsf; blue: 20 mbsf). (top) Bathymetry measured from CTD sensor in EM system.

sensor shows a response similar to the one previously observed in lines crossing the large pockmark P2, line 1 (Figure 5), although not as extensive (500 m wide between 2.7 and 3.2 km in profile). This area is located immediately adjacent to the igneous anomaly described previously, suggesting that the edges of the intrusion have been used as a path for fluid expulsion crossing sediment layers.

We also identify the central area in the profile (2.2–3.1 km in profile) as corresponding to region C. Here the conductivity data also show a complex structure and a drop of conductivity.

5.2.5. Line B

Line B (Figure 9) starts in the deepest part of the basin and follows a NW-SE direction, reaching the Malin Terrace on the SE of the study area. The conductivity profile along line B is typical of the Malin shelf. Conductivities are high in the deepest part of the basin and decreases toward the basin edge. The data suggest a well-preserved layering of the sediments, except within the anomalous area associated with the magmatic intrusion and pockmark 2. Toward the end of the profile, both conductivity curves separate, indicating a change in facies as the instrument leaves the basin.

As in previous profiles, we can also identify region C in this profile (approximately from 2 to 4 km in the profile), with the same characteristics: complex structure and a drop in conductivity from the surrounding values.

5.2.6. Line C

Line C (Figure 10) crosses the eastern side of the basin. The conductivities recorded by both receivers start at around 0.9 S/m and follow a similar, parallel trend. This line displays an increasing trend of the conductivity as the instrument moved northeastward into the basin, corresponding to a decrease of the grain size (larger amounts of silt) in the sediments within the basin. Toward the end of the profile the instrument crossed a large pockmark (feature P1 in Figures 2 and 10). Here the responses from both receivers show a drop in conductivity. The bathymetry (Figure 10, top plot) indicates that along the crossing line, pockmark 1 (P1 in Figure 2) is composed of at least two fluid escape features; this also corresponds to the two minima that are observed on the shallow receiver.

In this profile regions, E, D, and C as they were defined in line 1, can also be seen. In particular, providing an extension to the NE of region C.

5.3. Characterization of the Inner Basin

Based on the conductivity sections extracted from the EM profiles, we can define an inner basin, within the Malin basin itself, coincident with the area containing the majority of the large pockmarks associated with the Skerryvore Fault (Figure 2). This region has been defined using primarily line 1 data, but also lines 3, A, B, and C. This inner basin is an elongated feature running from the SW to the NE, with a width of 2–4 km. Our data are unable to constrain its length but it is likely at least several kilometers long (Figure 11). This inner basin is marked by a gentle increase of conductivities around the edges. The interior of this inner basin is marked by a drop in conductivities, displaying homogeneous values disrupted only by anomalies marking the presence of edges of pockmarks or subsurface gas accumulation (Figures 5 and 7–10). This feature was termed the Malin Deep micro basin in *Szpak et al.* [2012], but since in the present work we can map its extension to a few kilometers we prefer to call it the inner basin.

The above mentioned drop in conductivity values within the pockmark is confirmed by sediment core analysis results (Tables 1 and 2 and Figures 3 and 4). The main difference observed between both cores is that core CE08_044 (outside the pockmark) shows, according to physical properties logs, distinct stratigraphic units, whilst core CE08_045 (inside the pockmark) shows no layering and very homogeneous physical properties. Furthermore, the analysis shows that outside the pockmark (core CE08_044, Table 1) the mean grain size is, on average, coarser than within the pockmark (core CE08_045, Table 2) by 36%, clay content is lower (3% versus 13%) and there is a lower degree of sorting (1.5 versus 2.3).

The inner basin region (region C, Figures 5 and 7–10) has been defined from EM conductivity values, although analyses of the cores confirm changes in the homogeneity of sediments. This inner basin includes
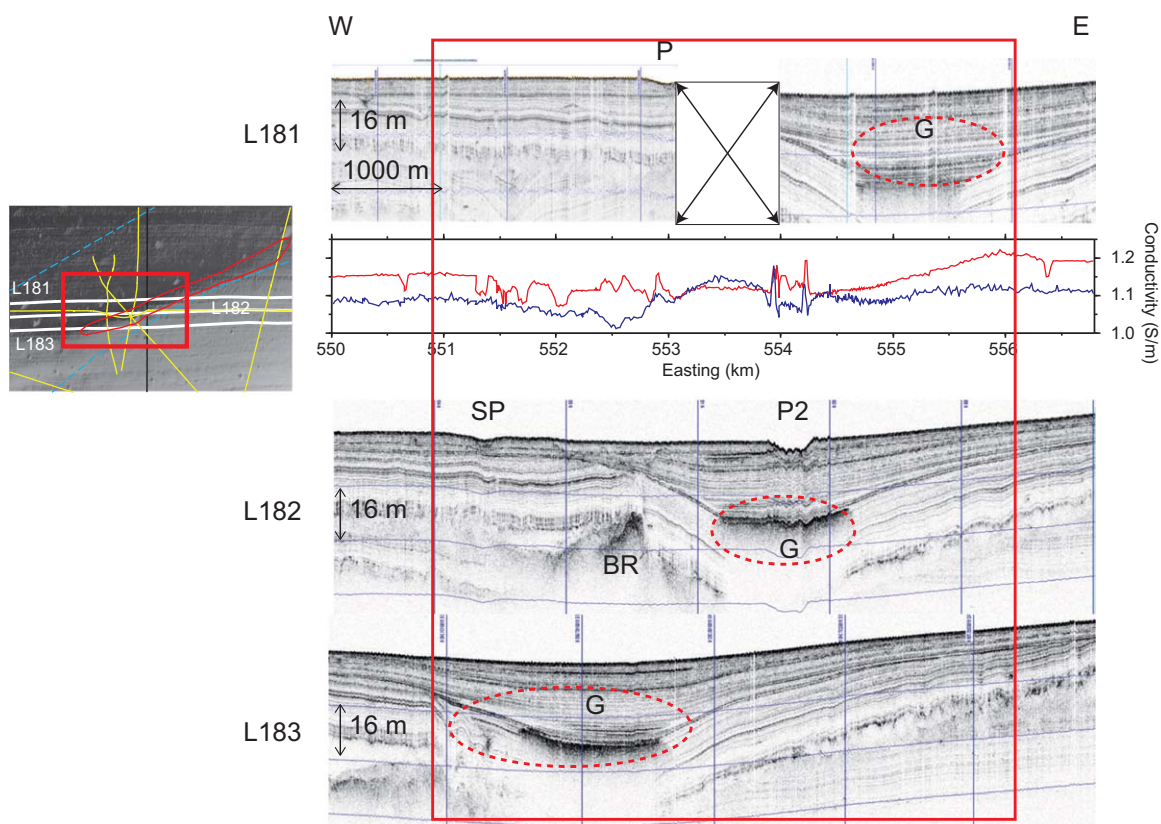

Figure 11. Gas anomalies in the central part of the basin as observed in the EM (line 1) and 3 parallel shallow seismic lines (181, 182, and 183). The enhanced reflectors interpreted as gas accumulation facies (G) are present in the three parallel lines and coincide with the edges of the EM gassy region (C). SP is a small pockmark, see also Figure 5. BR refers to a bright reflector interpreted as a magmatic intrusion.

the area affected by pockmarks, but the changes are not inherent to the pockmark area but are present throughout. The inner basin is also the area more affected by pockmarks [*Monteys et al.*, 2008] and can be associated with the Skerryvore Fault. The largest geophysical differentiation in this inner basin is found in the superficial part, as the shallow EM receiver is more affected than the deeper one. In general, this area is characterized by reduced and more irregular conductivity values.

Figure 11 shows SBP (subbottom profiler) lines 181, 182, and 183, together with EM Line 1 (see also Figure 2 for geographical location). The most striking feature on these plots is the area with gas accumulation, coincident with the inner basin anomalous conductivity response (region C). This feature runs in a WSW-ENE direction and correlates well with the inferred position of the Skerryvore Fault (Figure 2). The seismic reflection line DBS99_128 (Figure 7), delineates the North-South extend of region C, marked by the presence of a channel-like feature, which is limited to the central part of the basin and is not a regional feature.

6. Discussion

The EM data show an increase in conductivity toward the center of the Malin basin that suggests higher porosities within sediments. We interpret this as the regional trend within the Malin basin. Across the basin, the EM data show numerous anomalies that are associated with the presence of gas or freshwater, also seen in the shallow seismic records (see Figure 11). Core sample analysis confirms differences in sediment composition inside and outside of the pockmark. The central part of the basin is characterized by a NE-SW elongated conductive anomaly, which is defined by a sharp decrease in the conductivity with respect to the adjacent areas of the basin. This anomalous conductivity region correlates well with the NE-SW surface expression of the Skerryvore Fault and fluid escape features observed in the acoustic records.

Local high-conductivity anomalies in the vicinity of the pockmarks could have been caused by gas-fueled increase in microbial activity [*Szpak et al.*, 2012], as it has been shown that such activity can affect geo-electrical properties of sediments [*Atekwana et al.*, 2004; *Abdel Aal et al.*, 2010] (see, for example, in Figure 5 the area located under pockmark 2). *Szpak et al.* [2012] show geochemical signatures of microbial activity from analysis of the cores also used in this work. Similar local anomalies have been observed in several of the EM lines and are confirmed by crossovers. Although the geochemical evidence points toward microbial activity, some of these anomalies could also be caused by changes in sediment permeability resulting from fluid flow.

In particular, 1 km West of pockmark 2 (Figure 5) there is an area of enhanced reflectivity that we interpret as presence of gas in the strata, which corresponds to an increase of conductivities in the 40 m (deeper) receiver. As mentioned earlier, the expected response of the EM system to the presence of gas is the opposite. Geochemical analysis of the core in this area [*Szpak et al.*, 2012] shows evidence of microbial activity, which can affect the conductivity of sediments as mentioned above.

According to *Judd and Hovland* [2007], while the initial pockmark formation has a blowout like characteristic, later fluid migration is likely to use already existing pathways. More recent studies [*Hovland et al.*, 2010], suggest that fluids escape gradually while the reservoir is charging. Once the gas in the reservoir is sufficient overpressured, it will push through the geological seal. The acoustic data in Figure 5 show areas of blanking or interruption of the layering from the surrounding areas under the pockmark, this has been interpreted as the result of sediment mixing and of pockmark formation. The meaning of this vertical acoustic blanking is still poorly understood and widely debated [*Judd and Hovland*, 2007]. This is also observed in the core analysis (Tables 1 and 2 and Figures 3 and 4), where the core taken from within the pockmark shows a more homogeneous layering in comparison to the core from outside the pockmark where a distinct layering is observed.

Core data analysis from outside the pockmark (core CE08_044, Figure 3 and Table 1) shows a well-preserved layering with a sand-rich unit between 1.5 and 3 mbsf. The conductivity in this region (see Figure 5), as measured by the shallow EM receiver, is low compared to values obtained elsewhere within the basin. The core inside the pockmark (core CE08_045, Figure 4 and Table 2) shows nonlayered, sedimentary structure with no apparent sediment grain size gradients, typical of reworked material, and the EM data show a regional trend in conductivity (Figures 5, 7, and 9). Apparent conductivities are larger than outside the pockmark. *Szpak et al.* [2012] have associated the increase in conductivity within the pockmark with bacterial activity. These observations suggest

that there is a large amount of gas in the sediments of the basin, but within the pockmarks (1) gas has escaped and sediments have been disturbed, thus increasing the porosity, and (2) there is a higher level of bacterial activity. Both of these phenomena can explain the difference in conductivity between the pockmark and the basin. Additionally, shallow structures in the SBP data (Figures 5 and 11) are more disturbed than the deeper parts, possibly indicating that gas has accumulated in the upper strata.

The edges of the pockmark are associated with narrow positive conductive anomalies. *Newman et al.* [2008] have pointed out that methane venting from a large pockmark in the Atlantic coast of the United States occurs along the upper parts of the pockmark walls and is not occurring through the floor of the pockmark. *Chatterjee et al.* [2011] report that increased fluid flux and deep source methane input result in enhanced concentrations of hydrate and free gas that accumulate on areas of larger porosity. With the help of all these observations, we can interpret the conductivity anomalies observed across pockmarks. The internal part of the pockmark has a decrease of conductivity because of the presence of gas and the more heterogeneous structure of the sediments. As sedimentation is responsible for deposition of organic material, venting provides chemical energy, in areas of active seeping microbial communities thrive [*Jørgensen and Boetius*, 2007]. While the walls of the pockmark constitute pathways for fluid release and hence likely have higher permeability and porosity from disturbed sediments, and therefore higher conductivity, we believe that this location is also where most microbial activity concentrates. Following the results of *Atekwana et al.* [2004], there is probably an added increase of the conductivity associated with this microbial activity, although a detailed ground-truthing study would be required to assess this. At the same time, around these walls there is an accumulation of free gas that causes a conductivity decrease.

Not all the conductivity anomalies caused by presence of gas are the same. Large pockmarks appear as sharp conductivity anomalies (positive in the walls and negative in the center) and gas charged areas display a large regional trend. This is clearly observed in line C (Figure 10), as the instrument enters the basin both measurements of conductivity rise until the instruments entered a pockmark. Sediments charged with gas should generally show a decrease in their conductivity, as has been seen elsewhere [*Hsu et al.*, 2014]. The results shown in Figure 10 can be interpreted as a (1) change in sediment facies, with coarser sands outside the basin and finer, muddy sediments in the interior [*Monteys et al.*, 2008], (2) in certain locations, the presence of microbial activity that is known to increase the conductivity of sediments [*Atekwana et al.*, 2004], and (3) caused by the water influx as gas has been released refilling sediment pores [*Sultan et al.*, 2011], which will cause an increase of conductivity as the resistive phase (gas) is removed from sediments. In the case of a change in facies, we need to consider that gas will be very well distributed in sand within the matrix, decreasing the effective conductivity of sediments, but in the case of mud, with higher permeability, gas is trapped in layers, and is not as effective at decreasing the overall conductivity.

The upper section (top meter) combined results of the grain size and physical properties descriptors on the two cores suggest that part or most of the surface material within the pockmark has been reworked, possibly as a consequence of pockmark formation [*Judd and Hovland*, 2007]. Commonly during formation, pockmarks are left with so-called lag deposit which is usually coarser than surrounding seabed. This is due to the fines being suspended in the water column during venting/blowout and carried away from the site by currents while coarse particulates with lower sedimentation rates are deposited [*Judd and Hovland*, 2007]. A second plausible mechanism, topographic depressions can act as sediment traps retaining the coarser fraction while fine grains remain suspended in the water column. Both of these mechanisms are not exclusives and can act at times simultaneously.

While the general electrical properties of the basin are controlled by grain size, region C (the inner basin in Malin) has a very distinct electrical signature, which from the evidence in the conductivity anomalies, the SBP profiles and ground truthing, is marked by the presence of fluids, most likely gas and water released by sediment compaction.

The EM line 3, which crosses the entire basin from South to North, shows the largest conductivity variations (Figure 7). The Northern part (feature X) has large conductivity anomalies that correlate with presence of gas enhanced reflectors and a high density of pockmarks in coarser sediments, indicating fluid escape. Following the results, we have observed in other areas of the Malin Sea, it seems that microbial activity is the cause of this enhanced conductivity. Without a more thorough ground truthing we cannot ascertain the extent of possible microbial activity.

7. Conclusions

The general trend of the EM survey across the basin shows a gradual increase of conductivity toward the central and deepest part of the basin. Shallow seismic profiles and MBES observations also reflect sedimentary changes across the basin, in a fairly homogenous sediment stratum.

Electromagnetic surveys across the Malin Basin show a number of conductivity anomalies associated with the presence of gas charged sediments in the upper strata. These anomalies consist in a general increase in conductivity over the areas with a higher density of gas reflectors and with local sharp increments (peaks). This correlates well with gas related echo facies as observed in the sub bottom records.

Although the observation of higher conductivities with highest volumes of gas seems counter intuitive, the geophysical signatures correspond to changes in sediment grain size ranging from fairly homogeneous sands to clays, indicating changes in porosity control the conductivity rather that gas.

There are EM signatures that appear as positive anomaly changes in conductivity compared to the surrounding trend. These have been observed both as local peaks and also as kilometer long high-conductivity anomalies. We interpret these anomalies as fluid accumulation parallel to the strata, which are well correlated to enhanced amplitude reflectors in the subbottom profiler records.

There are some local anomalies characterized by short intervals of lower conductivity, which could either be caused by gas associated with vertical migration pathways or local disruption of the shallow strata produced by fluid disturbance. While the former shows the expected conductivity response decrease caused by the presence of free gas in sediments, the latter would be related to a decrease due to the layer discontinuity, as observed in the shallow seismic records.

The areas corresponding to the pockmark depression are characterized in general by high-conductivity peaks at the edges, while inside the unit the conductivity drops and is fairly homogeneous, as well as in the vicinity of the pockmark. The lower conductivity values across the pockmark depression are found inside the unit pockmarks. Sediment core data suggests that within the two pockmark units studied certain strata show evidence of increased microbial activity [*Szpak et al.*, 2012], which in turn can increase bulk electrical conductivities as pointed out by *Atekwana et al.* [2004].

References

Abdel Aal, G. Z., E. A. Atekwana, and E. A. Atekwana (2010), Effect of bioclogging in porous media on complex conductivity signatures, *J. Geophys. Res.*, *115*, G00G07, doi:10.1029/2009JG001159.

Anderson, A. L., and L. D. Hampton (1980), Acoustics of gas–bearing sediments I. Background, *J. Acoust. Soc. Am.*, *67*(6), 1865–1889, doi: 10.1121/1.384453.

Archie, G. E. (1942), The electrical resistivity log as an aid in determining some reservoir characteristics, *Trans. Am. Inst. Min. Metal. Eng.*, *146*, 54–67.

Atekwana, E. A., D. D. J. Werkema, J. W. Duris, S. Rossbach, E. A. Atekwana, W. A. Sauck, D. P. Cassidy, J. Means, and F. D. Legall (2004), In-situ apparent conductivity measurements and microbial population distribution at a hydrocarbon-contaminated site, *Geophysics*, *69*(1), 56–63, doi:10.1190/1.1649375.

Börner, J. H., V. Herdegen, J.-U. Repke, and K. Spitzer (2013), The impact of CO_2 on the electrical properties of water bearing porous media: Laboratory experiments with respect to carbon capture and storage, *Geophys. Prospect.*, *61*(s1), 446–460, doi:10.1111/j.1365-2478.2012.01129.x.

Chatterjee, S., G. Gu, W. G. Chapman, G. J. Hirasaki, G. Bhatnagar, B. Dugan, and G. R. Dickens (2011), Effects of heterogeneous lithology and focused fluidflow on gas hydrate distribution in marine sediments, paper presented at 7th International Conference on Gas Hydrates (ICGH 2011), Scotland, U. K.

Cheesman, S. J. (1989), *A Short Baseline Transient Electromagnetic Method for Use on the Sea Floor*, edited by S. J. Cheesman, Univ. of Toronto, Dep. of Phys., Geophys. Lab., Toronto, Ontario.

Cheesman, S. J., L. K. Law, and B. St. Louis (1993), A porosity mapping survey in Hecate Strait using a seafloor electro-magnetic profiling system, *Mar. Geol.*, *110*(3–4), 245–256, doi:10.1016/0025-3227(93)90087-C.

Dobson, M. R., and D. Evans (1974), Geological structure of the Malin Sea, *J. Geol. Soc. London*, *130*(5), 475–478, doi:10.1144/gsjgs.130.5.0475.

Dobson, M. R., and R. J. Whittington (1992), Aspects of the geology of the Malin Sea area, *Geol. Soc. Spec. Publ.*, *62*(1), 291–311, doi:10.1144/GSL.SP.1992.062.01.23.

Dorschel, B., A. Wheeler, X. Monteys, and K. Verbrugge (2011), Atlas of the Deep-Water Seabed: Ireland, Springer, London.

Dunlop, P., R. Shannon, M. McCabe, and R. Quinn (2010), Marine geophysical evidence for ice sheet extension and recession on the Malin Shelf: New evidence for the western limits of the British Irish Ice Sheet, *Mar. Geol.*, *276*(1–4), 86–99, doi:10.1016/j.margeo.2010.07.010.

Evans, D., R. J. Whittington, and M. R. Dobson (1985), *Tiree Solid Geology, 1:250,000 Scale (map), (Institute of Geological Sciences)*, British Geological Survey, Nottingham (UK).

Evans, R. L. (2001), Measuring the shallow porosity structure of sediments on the continental shelf: A comparison of an electromagnetic approach with cores and acoustic backscatter, *J. Geophys. Res.*, *106*(C11), 27,047–27,060, doi:10.1029/2000JC000487.

Evans, R. L. (2007), Using CSEM techniques to map the shallow section of seafloor: From the coastline to the edges of the continental slope, *Geophysics*, *72*(2), WA105, doi:10.1190/1.2434798.

Evans, R. L., and D. Lizarralde (2003), Geophysical evidence for karst formation associated with offshore groundwater transport: An example from North Carolina, *Geochem. Geophys. Geosyst.*, *4*(8), 1069, doi:10.1029/2003GC000510.

Evans, R. L., L. K. Law, B. St. Louis, S. J. Cheesman, and K. Sananikone (1999), The shallow porosity structure of the Eel shelf, northern California: Results of a towed electromagnetic survey, *Mar. Geol.*, *154*(1–4), 211–226, doi:10.1016/S0025-3227(98)00114-5.

Fleischer, P., T. Orsi, M. Richardson, and A. Anderson (2001), Distribution of free gas in marine sediments: A global overview, *Geo Mar. Lett.*, *21*, 103–122, doi:10.1007/s003670100072.

Floodgate, G., and A. Judd (1992), The origins of shallow gas, *Cont. Shelf Res.*, *12*(10), 1145–1156, doi:10.1016/0278-4343(92)90075-U.

Fonseca, L., L. Mayer, D. Orange, and N. W. Driscoll (2002), The high-frequency backscattering angular response of gassy sediments: Model/data comparison from the Eel River Margin, California, *J. Acoust. Soc. Am.*, *111*(6), 2621–2631, doi:10.1121/1.1471911.

Garcia, X., X. Monteys, R. L. Evans, and B. Kelleher (2007), Geohazard identification and early reconnaissance for hydrocarbon potential using marine electromagnetic and high frequency acoustic methods, *Geophys. Res. Abstr.*, *9*, 09524, 16–20, SRef-ID: 1607-7962/gra/EGU2007-A-09524.

Hovland, M. (1984), Gas-induced erosion features in the north sea, *Earth Surf. Processes Landforms*, *9*, 209–228.

Hovland, M., and A. Judd (1988), *Seabed Pockmark and Seepages: Impact on Geology, Biology and the Marine Environment*, 293 pp., Graham and Trotman, London.

Hovland, M., R. Heggland, M. De Vries, and T. Tjelta (2010), Unit-pockmarks and their potential significance for predicting fluid flow, *Mar. Pet. Geol.*, *27*(6), 1190–1199, doi:10.1016/j.marpetgeo.2010.02.005.

Hsu, S. K., C.-W. Chiang, R. L. Evans, C.-S. Chen, S.-D. Chiu, Y.-F. Ma, S.-C. Chen, C.-H. Tsai, S.-S. Lin, and Y. Wang (2014), Marine controlled source EM method used for the gas-hydrate investigation in the area off SW Taiwan, *J. Asian Earth Sci.*, doi:10.1016/j.jseaes.2013.12.001, in press, http://www.sciencedirect.com/science/article/pii/S1367912013006202.

Jackson, P. D., D. T. Smith, and P. N. Stanford (1978), Resistivity–porosity–particle shape relationships for marine sands, *Geophysics*, *43*(6), 1250–1268, doi:10.1190/1.1440891.

Jackson, P. D., R. C. Flint, and K. B. Briggs (1998), Two- and three-dimensional heterogeneity in carbonate sediments using resistivity imaging, *J. Acoust. Soc. Am.*, *104*(3), 1812–1812, doi:10.1121/1.423422.

Jørgensen, B. B., and A. Boetius (2007), Feast and famine—Microbial life in the deep-sea bed, *Nat. Rev. Microbiol.*, *5*(10), 770–781, doi:10.1038/nrmicro1745.

Josenhans, H. W., L. H. King, and G. B. Fader (1978), A side-scan sonar mosaic of pockmarks on the Scotian shelf, *Can. J. Earth Sci.*, *15*(5), 831–840, doi:10.1139/e78-088.

Judd, A., and M. Hovland (2007), *Seabed Fluid Flow. The Impact on Geology, Biology, and the Marine Environment*, 492 pp., Cambridge Univ. Press, Cambridge, UK.

King, L. H., and B. MacLean (1970), Pockmarks on the Scotian Shelf, *Geol. Soc. Am. Bull.*, *81*(10), 3141, doi:10.1130/0016-7606(1970)81[3141:POTSS]2.0.CO;2.

Kvenvolden, K. A., and B. W. Rogers (2005), Gaia's breath—Global methane exhalations, *Mar. Pet. Geol.*, *22*(4), 579–590, doi:10.1016/j.marpetgeo.2004.08.004.

Milkov, A. V. (2000), Worldwide distribution of submarine mud volcanoes and associated gas hydrates, *Mar. Geol.*, *167*(1–2), 29–42, doi:10.1016/S0025–3227(00)00022-0.

Minshull, T. A., G. K. Westbrook, K. A. Weitemeyer, M. C. Sinha, B. K. Goswami, and B. Marsset (2012), Leaking Methane Reservoirs Offshore Svalbard, *Eos Trans. AGU*, *93*(42), 413–414, doi:10.1029/eost2012EO42.

Monteys, X., D. Hardy, E. Doyle, and S. Garcia-Gil (2008), Distribution, morphology and acoustic characterisation of a gas pockmark field on the Malin Shelf, NW Ireland, paper presented at OSP-01 General Contributions to Marine Geoscience and Paleoceanography Symposium, Int. Geol. Congr., Oslo.

Müller, H., T. von Dobeneck, W. Nehmiz, and K. Hamer (2011), Near-Surface EM, rock-magnetic, and geochemical fingerprinting of submarine freshwater seepage at Eckernförde bay, *Geo Mar. Lett.*, *31*(2), 123–140, doi:10.1007/s00367-010-0220-0.

Newman, K. R., et al. (2008), Active methane venting observed at giant pockmarks along the U.S. mid-Atlantic shelf break, *Earth Planet. Sci. Lett.*, *267*(1–2), 341–352, doi:10.1016/j.epsl.2007.11.053.

Parnell, J. (1992), Burial histories and hydrocarbon source rocks on the North West Seaboard, *Geol. Soc. Spec. Publ.*, *62*(1), 3–16, doi:10.1144/GSL.SP.1992.062.01.02.

Ren, S. R., Y. Liu, Y. Liu, and W. Zhang (2010), Acoustic velocity and electrical resistance of hydrate bearing sediments, *J. Pet. Sci. Eng.*, *70*(1–2), 52–56, doi:10.1016/j.petrol.2009.09.001.

Rice, D. D., and G. E. Claypool (1981), Generation, accumulation, and resource potential of biogenic gas, *AAPG Bull.*, *65*(1), 5–25.

Riddihough, R. (1968), Magnetic surveys off the north coast of ireland, *Proc. R. Irish Acad.*, *66*, 27–41.

Schubel, J. R. (1974), Effects of tropical storm agnes on the suspended solids of the northern chesapeake bay, in *Suspended Solids in Water, Mar. Sci., vol. 4*, edited by R. Gibbs, pp. 113–132, Springer, U.S., doi:10.1007/978-1-4684-8529-5_8.

Schwalenberg, K., E. Willoughby, R. Mir, and R. N. Edwards (2005), Marine gas hydrate electromagnetic signatures in Cascadia and their correlation with seismic blank zones, *First Break*, *23*, 57–63.

Sills, G. C., and S. J. Wheeler (1992), The significance of gas for offshore operations, *Cont. Shelf Res.*, *12*(10), 1239–1250, doi:10.1016/0278-4343(92)90083-V.

Sultan, N., et al. (2011), Dynamics of fault-fluid-hydrate system around a shale-cored anticline in deepwater Nigeria, *J. Geophys. Res.*, *115*, B08101, doi:10.1029/2011JB008218.

Szpak, M. T., X. Monteys, S. O'Reilly, A. J. Simpson, X. Garcia, R. L. Evans, C. C. R. Allen, D. J. McNally, D. Courtier-Murias, and B. P. Kelleher (2012), Geophysical and geochemical survey of a large marine pockmark on the Malin Shelf, Ireland, *Geochem. Geophys. Geosyst.*, *13*, Q01011, doi:10.1029/2011GC003787.

Taylor, D. (1992), Nearshore shallow gas around the U.K. coast, *Cont. Shelf Res.*, *12*(10), 1135–1144, doi:10.1016/0278-4343(92)90074-T.

Wessel, P., and W. H. F. Smith (1991), Free software helps map and display data, *Eos Trans. AGU*, *72*, 441–446.

Wilkens, R., and M. Richardson (1998), The influence of gas bubbles on sediment acoustic properties: In situ, laboratory, and theoretical results from Eckernförde bay, Germany, *Cont. Shelf Res.*, *18*, 1859–1892.

Wilt, M., and D. Alumbaugh (1998), Electromagnetic methods for development and production: State of the art, *Leading Edge*, *17*(4), 487–487.

Yuan, F., J. D. Bennell, and A. M. Davis (1992), Acoustic and physical characteristics of gassy sediments in the western Irish Sea, *Cont. Shelf Res.*, *12*(10), 1121–1134, doi:10.1016/0278–4343(92)90073-S.

Yuan, J., and R. N. Edwards (2000), The assessment of marine gas hydrates through electrical remote sounding: Hydrate without a BSR?, *Geophys. Res. Lett.*, *27*(16), 2397–2400, doi:10.1029/2000GL011585.